# Spatial correlation of deuteron ordering in the glass phase of $Rb_{0.5}(ND_4)_{0.5}D_2PO_4$

N. Korner and R. Kind
*Institute of Quantum Electronics, ETH-Hönggerberg, CH 8093 Zürich, Switzerland*
(Received 29 July 1993)

We have investigated the extent of the spatial correlation of deuteron ordering in the solid solution $Rb_{1-x}(ND_4)_xD_2PO_4$ (D-RADP-$X$, $X=100x$) by means of quadrupole-perturbed $^{87}Rb$ NMR. In contrast to the usual approach where glass transitions are discussed in terms of a departure from complete disorder, we are treating the ordering in D-RADP-$X$ as a departure from the long-range-ordered ferroelectric (FE) and antiferroelectric (AFE) phase states. The composition parameter $x$ is a parameter for the competing FE and AFE interactions which reduces the spatial correlation length of the ordered phases to the nanometric region ($0.35<x<0.56$). This approach allows us to make use of techniques employed in the classical distortive phase transitions and to expand them to short-range correlated systems. The results of this analysis clearly show that the glass state of D-RADP-50 consists of short-range-ordered AFE clusters of an average size 6 to 8 $nm^3$: i.e., a correlated order of about 150–200 O-D $\cdots$ O bonds. This size is too small to exhibit features of the long-range-ordered AFE phase state, such as a phase transition with a well-defined transition temperature. Nevertheless, this local order can be distinguished unambiguously from a random freeze-out of the deuterons in the O-D $\cdots$ O bonds.

## I. INTRODUCTION

The translational invariance of a regular crystal lattice of infinite size is used widely in solid-state physics. It enables the description of lattice vibrations by means of modes and the symmetry of their eigenvectors which transform according to irreducible representations of the system space group. As another example, the Landau theory of structural phase transitions requires for a continuous transition that the displacement eigenvector of the order parameter transforms like a symmetry-breaking irreducible representation of the space group the system takes on above the transition temperature $T_c$. These two concepts are the basis of the "soft-mode" theory; i.e., the connection of the order parameter with a low-lying symmetry-breaking phonon branch.

Any violation of the translational invariance, for example, by defects, substitutional disorder (in particular if competing interactions are introduced), incommensurate modulation, glassy-type ordering, etc., affects the applicability of the above-mentioned concepts. As a result, instead of a perfect symmetry the system has an average symmetry only, instead of sharp eigenfrequencies it may have a quasicontinuous distribution of eigenfrequencies, instead of infinite spatial correlation lengths, a distribution of rather short finite correlation lengths. Sensitive indicators of such violations are phase transitions. For this reason, the phase transitions of strongly disordered systems became of great interest in the past decade. While macroscopic measurement techniques (measurements with wave vector $q=0$) yield information on perfect crystal lattices, the interpretation of the results becomes more cumbersome for strongly disordered systems, as a consequence of the partial breakdown of translational invariance. It is therefore essential to use also microscopic techniques such as NMR, x-ray and neutron scattering, and atomic force microscopy, which yield information on the local properties of the system.

The solid solution $Rb_{1-x}(NH_4)_xH_2PO_4$ and its deuterated analog $Rb_{1-x}(ND_4)_xD_2PO_4$, henceforth designated as RADP-$X$ and D-RADP-$X$ ($X=100x$), respectively, are good examples for studying the breaking of the translational invariance due to the random substitutional disorder between Rb and $NH_4$ which leads to competing ferroelectric (FE) and antiferroelectric (AFE) interactions. Recently, we have reported a detailed phase diagram of D-RADP-$X$ based on NMR results.[1] At low temperatures ($T<50$ K), we can distinguish between five different phase states: (i) $0\le x\le 0.2$, a complete FE long-range order, (ii) $0.2\le x\le 0.35$, phase segregation into long-range-ordered FE regions and glassy ordered regions, (iii) $0.35\le x\le 0.65$, only short-range glass order, (iv) $0.65\le x\le 0.75$, the AFE relaxor phase, (v) $0.75\le x\le 1.0$, AFE long-range order.

The phase diagram of RADP-$X$ and D-RADP-$X$ was first investigated by Courtens,[2] who has postulated the absence of long-range order at low temperatures in a certain composition range, i.e., the glassy type of ordering. This had initiated several studies of this system; for a review see Höchli, Knorr, and Loidl.[3] However, a real breakthrough in understanding was achieved when the pseudospin random-bond–random-field model of Pirc and co-workers[4,5] was introduced to explain the NMR line shapes of the acid deuterons in D-RADP-44,[6] as well as the $Tl^{2+}$ ESR line shapes of Tl-doped RADP-70.[7] This analysis revealed unambiguously the glassy character of the material, and confirmed the thermally activated dynamics observed in earlier $T_1$ measurements.[8,9] A further proof of the glassy character was the observation of a bifurcation between the field-cooled and zero-field-cooled static dielectric susceptibility in D-RADP-60 at 61 K.[10]

The Edwards-Anderson order parameter $q_{EA}$ defined in the model of Refs. 4 and 5, which can be written as the

 

second moment of the probability distribution function of the time-averaged local polarization $p$ as

$$q_{EA}=\int_{-1}^{-1}W(p)p^2dp\ , \tag{1}$$

where

$$p=\frac{1}{\tau}\int_0^{\tau}p(t)dt,\quad -1<p<+1\ ,$$

cannot, by itself, distinguish between a random freeze-out and a locally correlated freeze-out of the protons or deuterons, respectively, in biased hydrogen bonds. The length over which the protons are coherently frozen in one out of the six Slater configurations,[11] without violating the ice rules, has been derived from the diffuse diffracted x-ray intensity in RADP. It is 2.0 nm at low temperatures.[12] This is longer than the average proton-proton distance, but shorter than the typical size of a conventional domain.

In this contribution we report on the observation of different spatial correlations of deuteron order in D-RADP-$X$ and how they can be discriminated by the $^{87}$Rb NMR line shape. The basic idea behind this method is the following. For the long-range FE and AFE transitions, all electrical-field-gradient (EFG) tensor elements at the Rb site depend only on the corresponding order parameters and are thus correlated, whereas a random freeze-out of the deuterons on the hydrogen bonds leads to uncorrelated Gaussian distributions of these elements. Thus, short-range correlation will yield qualitatively different results from the two above-mentioned asymptotic cases. In particular, we can show that the glass state of the system is characterized by a short-range correlation in the deuteron order, which is different from a simple superposition of FE and AFE orders.

## II. EXPERIMENT

The deuterated single crystals of D-RADP-$X$ were grown in a $D_2O$ solution of an appropriate mixture of the two components D-RDP and D-ADP.[13] The degree of deuteration was better than 99% as determined from proton NMR. The resulting composition of the samples was checked at $T=300$ K by determining the $^{87}$Rb quadrupole coupling constant $e^2qQ/h=V_{ZZ}$ (where $V_{ZZ}$ is the largest element of the electric-field-gradient tensor $\partial^2V/\partial x_i\partial x_j$ in its principal axis system). The coupling constant $V_{zz}$ [$V_{zz}=V_{ZZ}$ in the paraelectric (PE) phase of D-RADP] was found to depend linearly on the composition parameter $x$: $V_{zz}=a-bx$, where $a=9.7$ MHz, $b=3.31$ MHz, and $x$ is the molar fraction of the D-ADP in the solution [Fig. 1(a)]. The NMR lines are inhomogeneously broadened, i.e., we have a Gaussian distribution of $V_{ZZ}$ with a standard deviation $\sigma_{ZZ}$ which depends on $x$ as $\sigma_{ZZ}(x)=2\sigma_{ZZ}(x=0.5)\sqrt{x(1-x)}$ [Fig. 1(b)], with $\sigma_{ZZ}(x=0.5)=0.75$ MHz, as suggested by numerical calculations.[14]

By measuring $V_{zz}$ for an unknown composition, $x$ can be determined with an accuracy of $\pm0.015$. Within this accuracy no systematic difference between the $x$ of the solution and the one of the growing crystal could be observed. The above-mentioned $x$ dependencies indicate that the system is homogeneous for the whole range of $x$ and does not show any sign of phase segregation, which would result in well-resolved values of $V_{zz}$ and not in its continuous Gaussian distribution around a mean value, which was observed.

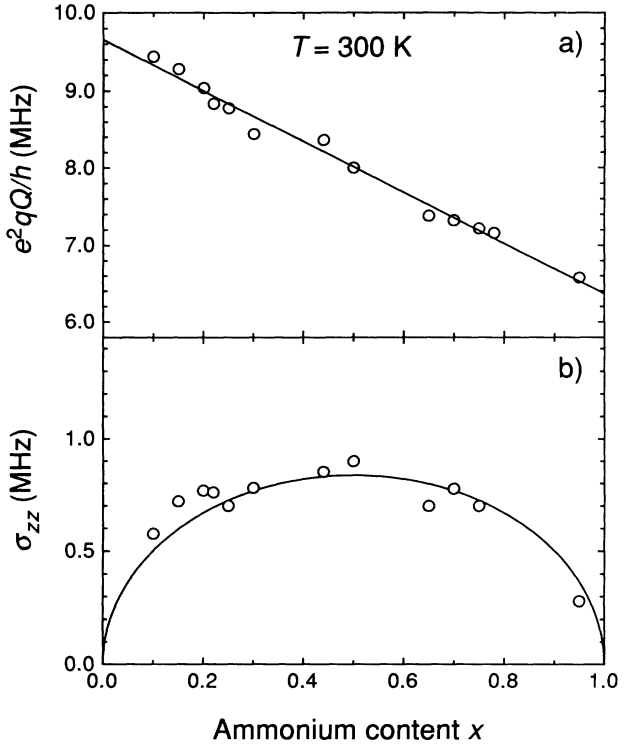


FIG. 1. (a) Nuclear quadrupole coupling constant $V_{zz}=e^2qQ/h$ and (b) its standard deviation $\sigma_{zz}$ for $^{87}$Rb in D-RDP-$X$ versus the $ND_4$ content $x$ of the solution out of which the samples were grown. The solid lines are calculated from the expressions given in the text.

The measurements were made with a home-built double-conversion spectrometer with intermediate frequencies of $I_1=145$ MHz and $I_2=15$ MHz in an external magnetic field $\mathbf{B}_0$ of 7 T. The temperature was stabilized in a continuous-flow cryostat with an accuracy of about $\pm0.05$ K. For the automatic temperature readout a Pt100 ($T>70$ K) and a calibrated carbon-glass resistor ($T<70$ K) were used. The crystal rotation about an axis perpendicular to $\mathbf{B}_0$ was performed automatically by a computer-controlled stepper motor.

The inhomogeneously broadened spectra of the $^{87}$Rb $-\frac{1}{2}\leftrightarrow+\frac{1}{2}$ transition have been determined by Fourier transforming the spin echo after a $90_x$-$90_y$ pulse sequence. An appropriate phase-cycling scheme has been applied to eliminate quadrature detection errors[15] and unwanted coherences due to pulse imperfections. The 90° pulse length was less than 4 $\mu$s. To be able to extract the desired information from the measured spectra it was necessary to obtain the pure absorption spectra of rather broad lines. This requires very short high-power rf pulses to obtain a broad enough irradiation spectrum. The deviations due to the finite width of the irradiation spectrum

can be compensated numerically in the measured spectra.[16] Moreover, it is important to apply a linear frequency-dependent phase correction to remove the phase gradient resulting from the discrete Fourier transformation. Typical rotation patterns exhibiting the orientational dependence of the $^{87}$Rb NMR line shifts, as well as of the line shapes, for the different phases of the system are shown in Fig. 2.

## III. SYMMETRY CONSIDERATIONS CONNECTED WITH LONG-RANGE ORDER

Both end compounds, D-RDP (tetragonal modification) with D-ADP, have the same tetragonal space group $I\bar{4}2d$ at room temperature (RT) with two formula units in the primitive unit cell ($Z=2$). X-ray and NMR-NQR measurements[12,17,18] revealed that the

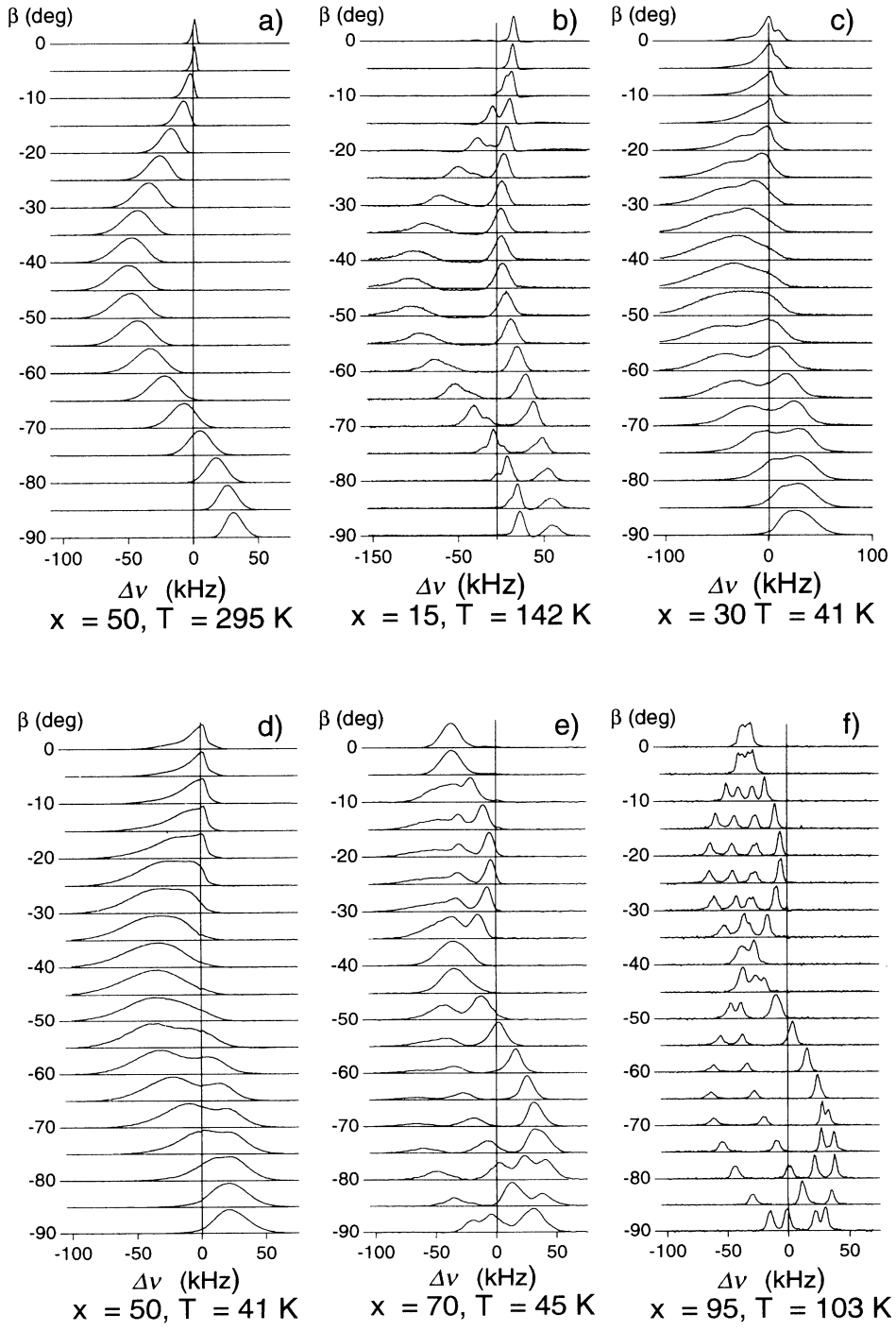


FIG. 2. Orientational dependence of the $^{87}$Rb $-\frac{1}{2}\leftrightarrow+\frac{1}{2}$ NMR spectra for various ammonium contents $x$ in the different phases of the D-RADP-$X$ system. The crystal has been rotated around the $a$ axis.

average structure is the same ($I\bar{4}2d$) for the whole composition range ($0 \le x \le 1$) at RT. The average site symmetry at the Rb position is $\bar{4}_z$. The average Rb EFG tensor is therefore given by

$$\mathbf{V}_0 = \bar{V}_{zz} \begin{bmatrix} -\frac{1}{2} & 0 & 0 \\ 0 & -\frac{1}{2} & 0 \\ 0 & 0 & 1 \end{bmatrix} . \tag{2}$$

This means $\bar{V}_{xz} = \bar{V}_{yz} = \bar{V}_{xy} = [\overline{(V_{xx} - V_{yy})} \equiv \bar{V}_\eta] = 0$. It was shown by means of model calculations[14] that the distributions of the five irreducible EFG tensor elements are uncorrelated Gaussians. These predictions were confirmed by $^{87}$Rb NMR.[8,17,19–21]

In the long-range-ordered FE phase of D-RADP the space group is $Fdd2$ with $Z = 2$. The site symmetry at the Rb position is reduced to $2_z$ and the EFG tensor at the Rb site can be expanded in terms of the FE order parameter $p_1$ ($-1 \le p_1 \le +1$):

$$\mathbf{V}_{\mathrm{FE}} = \mathbf{V}_0 + \begin{bmatrix} -\Delta V_\eta/2 & \Delta V_{xy} & 0 \\ \Delta V_{xy} & +\Delta V_\eta/2 & 0 \\ 0 & 0 & 0 \end{bmatrix} p_1 + \Delta V_{zz}^{(1)} \begin{bmatrix} -\frac{1}{2} & 0 & 0 \\ 0 & -\frac{1}{2} & 0 \\ 0 & 0 & 1 \end{bmatrix} p_1^2 + \cdots . \tag{3}$$

Here $p_1$ is a prefactor of the FE displacement eigenvector. The two Rb atoms in the primitive unit cell are related by the glide planes $d$. This symmetry operation changes the sign of $\Delta V_\eta$ in the first-order correction term. It is a well-known fact that the domain states occurring at the low-temperature side of a distortive phase transition are related by the lost symmetry elements of the point group ($\bar{4}_z, \bar{4}_z^3, 2_x, 2_y$). The first two correspond to a change of the signs of both $\Delta V_\eta$ and $\Delta V_{xy}$, while the latter two change the sign of $\Delta V_{xy}$ only. This leads to four different symmetry-related EFG tensors for the FE phase.

In the long-range-ordered AFE phase of D-ADP the space group is $P2_12_12_1$ with $Z = 4$ and there is no symmetry left at the $NH_4$ site. Thus all the elements $V_{xz}$, $V_{yz}$, $V_{xy}$, and $V_\eta$ are odd functions of the AFE order parameter $p_2$ ($-1 \le p_2 \le +1$). Here $p_2$ is a prefactor of one of the two AFE displacement eigenvectors. The selection of the eigenvector is determined within the matrix of the linear term in the following Eq. (4):

$$\mathbf{V}_{\mathrm{AFE}} \approx \mathbf{V}_0 + \begin{bmatrix} -\Delta V_\eta/2 & \Delta V_{xy} & \Delta V_{xz} \\ \Delta V_{xy} & +\Delta V_\eta/2 & \Delta V_{yz} \\ \Delta V_{xz} & \Delta V_{yz} & 0 \end{bmatrix} p_2 + \Delta V_{zz}^{(2)} \begin{bmatrix} -\frac{1}{2} & 0 & 0 \\ 0 & -\frac{1}{2} & 0 \\ 0 & 0 & 1 \end{bmatrix} p_2^2 + \cdots . \tag{4}$$

In our special case, measurements have shown[17] that the changes in $V_{xz}$ and $V_{yz}$ are so dominant that one can neglect the changes in $V_{xy}$ and $V_\eta$. The four $NH_4$ sites in the unit cell are related by the symmetry elements $2_x$, $2_y$, and $2_z$ which change the sign of $V_{xz}$, $V_{yz}$, or of both $V_{xz}$ and $V_{yz}$, respectively. The lost symmetry elements of the point group ($\bar{4}_z, \bar{4}_z^3, m_{xy}, m_{xy}^-$) relate the AFE domains. They all exchange $\Delta V_{xz}$ and $\Delta V_{yz}$ with alternating signs, which leads to eight different symmetry-related EFG tensors for the AFE phase.

It should be noted that (in contrast to the uncorrelated background distribution of the EFG tensor elements in D-RADP) Eqs. (3) and (4) show a pairwise correlation of the elements $\Delta V_{xy}, \Delta V_\eta$ and $\Delta V_{xz}, \Delta V_{yz}$, respectively. As a result, in the mixed-crystal system D-RADP we expect a superposition of both correlated and uncorrelated distributions of the EFG tensor elements at the Rb site. The resulting $^{87}$Rb ($I = \frac{3}{2}$) NMR spectra can be calculated from standard NMR-NQR theory[22–24], where the second-order shift of the central line ($-\frac{1}{2} \leftrightarrow +\frac{1}{2}$) is given by

$$\Delta\nu = \frac{1}{12\nu_L} \{ -2(\tilde{V}_{xz}^2 + \tilde{V}_{yz}^2) + \tfrac{1}{4}\tilde{V}_\eta^2 + \tilde{V}_{xy}^2 \} , \tag{5}$$

where $\nu_L$ is the Larmor frequency and the $\tilde{V}_{ik}$ are the EFG tensor elements in the coordinate system of the Zeeman interaction. They are obtained by a unitary transformation of the EFG tensor $\mathbf{V}$ in crystal coordinates,

$$\tilde{\mathbf{V}} = \mathbf{R}(\alpha,\beta,\gamma)\mathbf{V}\mathbf{R}(\alpha,\beta,\gamma)^{-1} . \tag{6}$$

If the external magnetic field $\mathbf{B}_0$ is oriented parallel to the $z$ axis of the crystal we have $\tilde{\mathbf{V}} = \mathbf{V}$ and one can see from Eq. (5) that FE ordering yields a positive frequency shift while AFE ordering yields a negative one, independent of the signs of the order parameters $p_1$ and $p_2$. When the crystal is then rotated about its $x$ axis for an angle $\beta$, the resulting frequency shift becomes for the paraelectric (PE) phase ($p_1 = p_2 = 0$)

$$\Delta\nu^{\mathrm{PE}}(\beta) = \frac{1}{12\nu_L} \tfrac{9}{16} V_0^2 [ -\tfrac{5}{8} - \tfrac{1}{2}\cos(2\beta) + \tfrac{9}{8}\cos(4\beta) ] . \tag{7}$$

In the case of FE ordering the frequency shift is

$$\Delta\nu^{\mathrm{FE}}(\beta) = \Delta\nu^{\mathrm{PE}}(\beta) + \frac{1}{12\nu_L} ( \tfrac{3}{16}\Delta V_\eta V_0 [ \tfrac{13}{4} - \cos(2\beta) - \tfrac{9}{4}\cos(4\beta) ] p_1 + \{ \tfrac{1}{2}\Delta V_{xy}^2 [ -1 + 3\cos(2\beta) ] + \tfrac{1}{32}\Delta V_\eta^2 [ \tfrac{11}{4} + 3\cos(2\beta) + \tfrac{9}{4}\cos(4\beta) ] \} p_1^2 ). \tag{8}$$

One can see that the linear term gives rise to a frequency splitting even for a single-domain crystal because of the glide

plane $d$ which changes the sign of $\Delta V_\eta$. For this rotation axis ($x$) the existence of FE domains does not lead to additional lines but for a general orientation of the $\mathbf{B}_0$ field up to four lines are expected.

The shift for AFE ordering is

$$\Delta\nu^{\mathrm{AFE}}(\beta)=\Delta\nu^{\mathrm{PE}}(\beta)+\frac{1}{12\nu_L}\left(\tfrac{3}{8}\Delta V_{yz}V_0[-\sin(2\beta)+\tfrac{9}{2}\sin(4\beta)]p_2\right.$$
$$+\{\tfrac{1}{2}\Delta V_{xz}^2[-1-3\cos(2\beta)]+\tfrac{1}{8}\Delta V_{yz}^2[-7-9\cos(4\beta)]$$
$$\left.+\tfrac{9}{8}\Delta V_{zz}^{(2)}V_0[-\tfrac{5}{8}-\tfrac{1}{2}\cos(2\beta)+\tfrac{9}{8}\cos(4\beta)]\}p_2^2\right) . \quad (9)$$

Note that the term containing $\Delta V_{zz}$ is of importance only for the antiferroelectric ordering ($\Delta V_{zz}^{(2)}\approx+1.8$ MHz, while $-\Delta V_{zz}^{(1)}<0.2$ MHz). The linear term leads to a frequency splitting for the single AFE domain since both symmetry elements $2_x$ and $2_y$ change the sign of $\Delta V_{yz}$. The occurrence of different AFE domains leads to additional line splitting since the lost symmetry elements exchange $V_{xz}$ and $V_{yz}$ as mentioned above. This also affects the quadratic term in Eq. (9). Thus, we have four NMR lines if the $\mathbf{B}_0$ field is in either the $x$-$z$ or the $y$-$z$ plane of the crystal, whereas for a general orientation eight lines are expected. This is in contrast to the findings in Ref. 25.

## IV. RELATION BETWEEN EFG TENSOR DISTRIBUTIONS AND NMR LINE SHAPES

The $^{87}$Rb NMR line shapes in D-RADP-$X$ are primarily the result of inhomogeneous quadrupolar broadening as the homogeneous contribution to the line width (due to $T_2$) is of the order of 0.5 kHz and can be neglected. Thus, the $^{87}$Rb NMR line shape is a homomorphous representation of the probability distributions of the five irreducible EFG tensor elements, according to Eqs. (5) and (6). The orientation dependence of the line shape resulting from the distribution of the EFG tensor elements is obtained from Eqs. (8) and (9) by setting $p_1$ and $p_2$ equal to unity and replacing the constants $\Delta V_{ij}$ by Gaussian random variables.

In this way the NMR line shape can be calculated exactly from the probability distributions of the EFG tensor elements in crystal coordinates for any crystal orientation in the external $\mathbf{B}_0$ field. The main task is thus to calculate these distributions for the various local orders of the hydrogen bonds within the observation range of the $^{87}$Rb nuclei. This observation range is an empirical parameter extracted from the point-charge model, which will be explained in more detail in Sec. V. It was first discussed in Ref. 14 in connection with the convergence of the charge-displacement model.

### A. Uncorrelated Gaussian distributions of the EFG tensor elements

In Ref. 14 it was shown that a random distribution of Rb and $NH_4$ in D-RADP leads to uncorrelated Gaussian distributions of the five irreducible EFG tensor elements at the site of the Rb nuclei. In a similar way one can show that a random freeze-out of the protons or deuterons in one of the two equivalent positions in the O-H $\cdots$ O bridges results also in uncorrelated Gaussian distributions of these elements. From this one can conclude that any static probability distribution of the local polarization $W(p)$ can create only a Gaussian distribution of the EFG tensor elements at the Rb site, provided there is no spatial correlation in the proton order.

For a general orientation of the external magnetic field $\mathbf{B}_0$ with respect to the crystal coordinate frame, the frequency shift $\Delta\nu(\beta,\delta,\varepsilon)$ can be written as

$$\Delta\nu(\mathbf{V},\beta,\delta,\varepsilon)=\sum_{i=1}^{5}a_{ij}(\beta,\delta,\varepsilon)V_i , \quad (10)$$

where $\beta$ is the running angle of the crystal rotation and $\delta$ and $\varepsilon$ describe the orientation of the rotation axis. The line-shape function $f(\Delta\nu)$ is given by

$$f(\Delta\nu)=\int\delta[\Delta\nu-\Delta\nu(\mathbf{V},\beta,\delta,\varepsilon)]P(\mathbf{V})d\mathbf{V}$$
$$=\int_{-\infty}^{+\infty}\exp(-i2\pi\Delta\nu t)G(t)dt , \quad (11)$$

where $G(t)=\int\exp[-i2\pi\Delta\nu(\mathbf{V},\beta,\delta,\varepsilon)t]P(\mathbf{V})d\mathbf{V}$. The symbol $\delta(x)$ is the Dirac delta function, $P(\mathbf{V})$ is the probability distribution function of the EFG tensor elements, and the Fourier-transform representation of $\delta(x)$ has been used. In a general situation, i.e., for correlation between different EFG tensor elements and $a_{ij}\neq0$ for $i\neq j$ in Eq. (10), the five-dimensional integral cannot be reduced to a simple analytical expression. In the special case where the crystal $c$ axis is parallel to the $\mathbf{B}_0$ field, the coefficients of the cross terms in Eq. (10) are zero, i.e., $a_{ij}=0$ for $i\neq j$. If one assumes uncorrelated Gaussian probability distributions ($P_G$) of the EFG tensor elements $P(\mathbf{V})=\prod_{i=1}^{5}P_G(V_i)$, $G(t)$ in Eq. (11) becomes

$$G(t)=\prod_{i=1}^{5}\left[\frac{\pi}{A_it+1/(2\sigma_i^2)}\right]^{1/2}$$
$$\times\exp\left\{\frac{\bar{V}_i^2}{2\sigma_i^2}\left[1+\frac{1}{A_it+1/(2\sigma_i^2)}\right]\right\} . \quad (12)$$

$\bar{V}_i$ and $\sigma_i^2$ are the first and second moments of the Gaussian probability distribution and $A_i=(2\pi i/12\nu_L)a_{ii}(\beta,\delta,\varepsilon)$. The homogeneous linewidth can be included by multiplying $G(t)$ by the $T_2$ decay $\exp(-t/T_2)$. Equation (11) can be fitted rather well to the measured line shape, Fig. 3.

For general situations the line-shape function $f(t)$ has

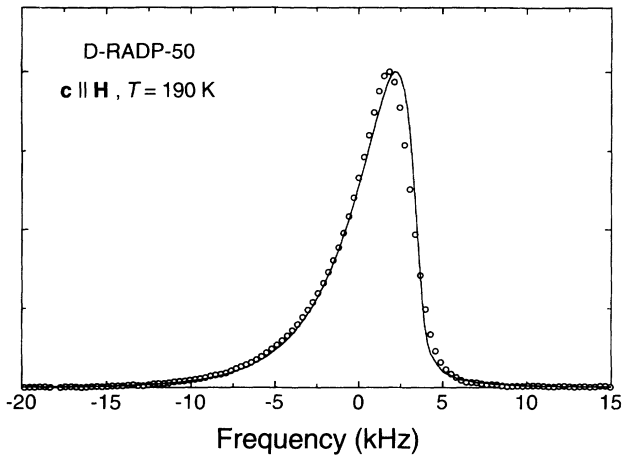


FIG. 3. $^{87}$Rb NMR-NQR line of the central transition in D-RADP-50 with $c\|\mathbf{H}$ and $T=190$ K. The solid line is a fit with the Fourier transform of Eq. (12).

to be determined by numerical methods. This is most easily done by a Monte Carlo procedure, where a random number generator is used to produce an EFG tensor. With Eqs. (7)–(9) the frequency shift $\Delta\nu$ is calculated and added up in a histogram. Figure 4 shows a Monte Carlo fit of excellent quality for the whole rotation pattern with

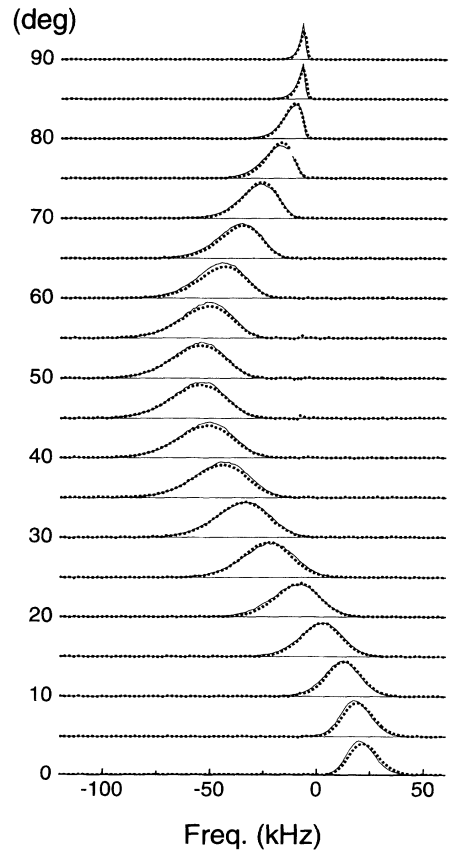


FIG. 4. Orientational dependence of the $^{87}$Rb NMR-NQR spectra in D-RADP-50 at $T=249$ K for a rotation around the crystal $a$ axis. The thick dashed lines are the measured spectra and the thin lines are fits with the Monte Carlo method.

a single set of parameters: $\overline{V_{zz}}$, $\sigma(V_{zz})$, $\sigma(V_{xz})$, $\sigma(V_{yz})$, $\sigma(V_\eta)$, $\sigma(V_{xy})$.

Another approach is based on an expansion of $\Delta\nu(\mathbf{V},\beta,\delta,\varepsilon)$ into a power series of $\delta V_i$'s to first order.[16–18] In the case of random $\delta V_i$'s with Gaussian probability distributions, the resulting frequency shift $\Delta\nu$ becomes a random variable with a Gaussian probability distribution as well. This approach is, of course, only useful for line shapes which are essentially Gaussian, which is not the case for certain orientations of the crystal is the $\mathbf{B}_0$ field for which the quadratic terms in Eqs. (7)–(9) become relevant. Nevertheless, this method gives reasonable values for the fit parameters which can be improved upon with the exact Monte Carlo method.

### B. Correlated Gaussian distributions

Correlated Gaussian distributions of the EFG tensor elements are obtained only in the presence of a spatial correlation of the proton or deuteron order. However, in this case the static probability distribution of the local polarization $W(p)$ must be Gaussian. This restriction is met in D-RADP-50 for temperatures above 150 K.[6] The pairwise correlation of the elements $\Delta V_{xy}$, $\Delta V_\eta$, and $\Delta V_{xz}$, $\Delta V_{yz}$, respectively, known for long-range order (Sec. III) is to be expected with smaller coefficients for the case of short-range correlation. In order to check this we have measured rotation patterns for the [1,1,0] axis at various temperatures. For this rotation axis, Eq. (9) has to be changed in the following way: $\Delta V_{xz}\rightarrow(\Delta V_{xz}+\Delta V_{yz})/\sqrt{2}$, $\Delta V_{yz}\rightarrow(\Delta V_{xz}+\Delta V_{yz})/\sqrt{2}$. Similarly one has to exchange $\Delta V_\eta$ and $2\Delta V_{xy}$ in Eq. (8). The variance of the new probability distribution $P(\Delta V_{xz}+\Delta V_{yz})/\sqrt{2}$ can be written as:

$$\sigma^2(P)=\tfrac{1}{2}\sigma^2(\Delta V_{xz})+\tfrac{1}{2}\sigma^2(\Delta V_{yz})+\mathrm{cov}(\Delta V_{xz},\Delta V_{yz})\ . \quad (13)$$

While the rotation patterns for the [1,0,0] and [0,1,0] axes depend on the pure variances $\sigma^2(\Delta V_{xz})$ and $\sigma^2(\Delta V_{yz})$ which are equal for symmetry reasons, the variance relevant for the [1,1,0] axis $\sigma^2(P)$ depends also on the correlation between the two distributions. According to Fig. 2 in Ref. 17 this should affect the [1,1,0] rotation pattern predominantly near $\beta=22°$ and $\beta=67°$. The lineshape fit for the whole rotation pattern, however, revealed that no covariance term is needed to describe the measured line shapes from room temperature to 150 K. Thus we can exclude any spatial correlation of the deuteron ordering for temperatures above 150 K. In this temperature range the static local polarization is due to a random field.

### C. Non-Gaussian EFG tensor distributions

The line shapes observed in the glass phase of D-RADP-50 [Fig. 2(d)] with their double-peaked structure for orientations around $\beta=65°$ and $\beta=25°$, can only be obtained from double-peaked probability distributions of some EFG tensor elements. As mentioned above, this can only occur in the presence of spatial correlation of the O-D $\cdots$ O deuteron ordering. From a comparison of

the rotation patterns of Fig. 2(d) (glass) with Fig. 2(b) (FE) and Fig. 2(f) (AFE) one can conclude that the correlation in the glass phase is essentially of AFE nature. A FE spatial correlation would exhibit the double-peaked structure mainly around $\beta=45°$ where the experimental line shape is, however, nearly Gaussian. Thus, a correlation between the distributions of $\Delta V_{xz}$ and $\Delta V_{yz}$ is to be expected that should be visible in the low-temperature rotation patterns for the [1,1,0] axis. However, these rotation patterns differ remarkably from Fig. 2(d), as in none of the orientations $\beta$ is a double-peaked line shape observed. This unambiguously proves the existence of AFE short-range correlation in the deuteron order. The onset of AFE short-range correlation below 150 K can also be observed in the temperature dependence of the average $^{87}$Rb NQ coupling constant $e^2qQ/h$, Fig. 5. The positive shift of about 0.6 MHz between the parallel high- and low-temperature slopes amounts to about $\frac{1}{3}$ of the spontaneous shift observed for AFE long-range ordering. Since the NMR line shapes can be calculated accurately for any set of probability distributions of the EFG tensor elements, we are faced with the problem of finding a suitable model for the calculation of these distributions from the probability distribution of the local polarization $W(p)$ according to the model calculations[4–6] by taking spatial short-range correlation into account.

## V. MODEL CALCULATIONS OF THE EFG TENSOR AT THE Rb SITE

Model calculations to study the influence of the static substitutional disorder on the distribution of the EFG tensor elements have been reported[14] for the RADP system. There it has been assumed that the substitution of a Rb atom by an ammonium group in pure RDP leads to a small lattice distortion around the $NH_4$ group, which results mainly in small displacements of the surrounding $PO_4$ groups. It was shown that a random distribution of Rb and $NH_4$ leads to uncorrelated Gaussian probability distributions of the EFG tensor elements. These "background distributions" are, of course, always present and have to be taken into account in any calculations. They are, however, temperature independent in the rigid-lattice model and thus their influence is important only at high temperatures, where $q_{EA}$ is small.

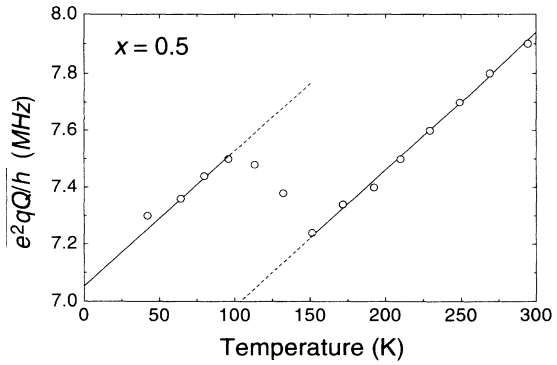


FIG. 5. Temperature dependence of the mean quadrupole coupling constant ($e^2qQ/h$) for $x=0.5$.

Here we use the same rigid-lattice point-charge model, but instead of the $NH_4$ shifts the displacements of the acid deuterons in the O-D $\cdots$ O bridges are considered. In the fast-motion regime, where the single-particle autocorrelation time $\tau_c \ll 1/|\Delta\omega_i|$ ($\Delta\omega_i$ is the NMR frequency shift induced by a jump of the $i$th deuteron), the time-averaged displacement of the deuteron from the center of the $i$th bond is given by:

$$\Delta r_i = 7.8\times10^{-2} p_i [\mathbf{r}(O_i^+) - \mathbf{r}(O_i^-)] , \tag{14}$$

where $p_i$ is the local polarization of the bond, according to Eq. (1), and the $\mathbf{r}(O)$ are the position vectors of the corresponding O atoms. The prefactor is given by half the distance between the two equilibrium positions of the deuterons divided by the bond length. Since the displacements are small compared with the distance of the deuterons from the origin, the change in the EFG tensor elements can be described by a linear expansion:

$$\Delta V_{jk} = \sum_{l=1}^{3} V_{jkl} \Delta x_l , \tag{15}$$

where the $\Delta x_l$ are the components of $\Delta\mathbf{r}_i$ and $V_{jkl}$ is given by

$$V_{jkl} = Q\left[ -\frac{15 x_j x_k x_l}{r^7} + \delta_{jl}\frac{3x_k}{r^5} + \delta_{kl}\frac{3x_j}{r^5} + \delta_{jk}\frac{3x_l}{r^5} \right] , \tag{16}$$

and $r_i = |\mathbf{r}(O_i^+) + \mathbf{r}(O_i^-)|/2$.

The lattice sum of the contributions $V_{jkl}$ converges rather rapidly with $1/r^2$.[14] It was taken for 288 O-D $\cdots$ O bonds or over 36 unit cells, respectively, ($\pm1.5$ lattice constants in the $x$ and $y$ directions and $\pm2$ in the $z$ direction). This proved to be sufficient since further increasing the number of unit cells did not affect the calculated EFG tensor elements. These numbers define the observation range of the Rb nucleus in the rigid-lattice approach. It should be noted that this observation range may be larger in the presence of elastic deformations.[14] For each run through the lattice one obtains one set of five irreducible $\Delta V_{jk}$. The probability distribution functions $P(\Delta V_{jk})$ are obtained by accumulating the results of about $10^4$–$10^5$ runs in histograms.

To describe the spatial correlation of the deuteron order we start with the six Slater configurations[11] (two FE and four AFE) under the assumption that the ice rules are respected throughout the whole crystal lattice, which is equivalent to enforcing translational invariance. For this case it is sufficient to describe the deuteron order for the AFE unit cell which contains eight O-D $\cdots$ O deuterons. This is shown in Fig. 6, where the eight bonds are numbered. The corresponding oxygen atoms are labeled with + or − signs to indicate their relative $z$ coordinates with respect to the center of the bond. For FE order with electric polarization in the positive $z$ direction, all deuterons are located in the potential wells close to the O(+) atoms. This defines also the sign of the corresponding local polarizations ($|p_i|=1$). Table I shows the local

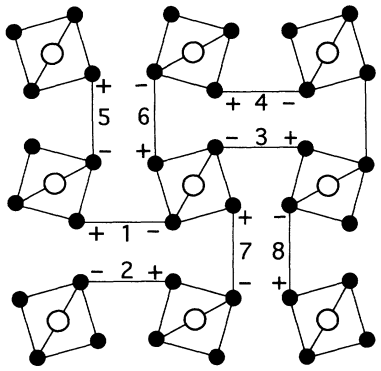


FIG. 6. Projection of the RDP structure along the $c$ axis. The ● represent the oxygen atoms of the $PO_4$ groups and the ○ correspond to the Rb and P positions, respectively. The hydrogen bonds are indicated by the lines connecting the $PO_4$ tetrahedra.

polarizations of the eight bonds for the six different Slater configurations.

The model calculations yield for the deviations $\Delta\mathbf{V}^{\mathrm{FE}}$ and $\Delta\mathbf{V}^{\mathrm{AFE}}$ (MHz) of the EFG tensor in the long-range-ordered FE and AFE phases,

$$\Delta\mathbf{V}^{\mathrm{FE}}=\begin{bmatrix}-3.70 & +1.45 & 0\\ +1.45 & +3.70 & 0\\ 0 & 0 & 0\end{bmatrix},$$

$$\Delta\mathbf{V}^{\mathrm{AFE}}=\begin{bmatrix}0 & 0 & -0.79\\ 0 & 0 & -4.18\\ -0.79 & -4.18 & 0\end{bmatrix}.$$

Since we do not want to make any assumptions concerning the quadrupole polarizability of the Rb atom and the effective charge of the hopping deuterons, we have scaled these results with a constant factor to match the measured and calculated values of $\Delta V_\eta$ of the FE phase.

From the experimentally determined EFG tensors of the long-range-ordered FE and AFE phase, one has to subtract the axially symmetric part to obtain the corresponding $\Delta\mathbf{V}^{\mathrm{FE}}$ and $\Delta\mathbf{V}^{\mathrm{AFE}}$:

$$\Delta\mathbf{V}^{\mathrm{FE}}_{\mathrm{expt}}=\begin{bmatrix}-3.70 & +0.65 & 0\\ +0.65 & +3.70 & 0\\ 0 & 0 & 0\end{bmatrix},$$

$$\Delta\mathbf{V}^{\mathrm{AFE}}_{\mathrm{expt}}=\begin{bmatrix}+0.57 & +0.69 & -2.32\\ +0.69 & -0.57 & -4.16\\ -2.32 & -4.16 & 0\end{bmatrix}.$$

The comparison shows that the model calculations yield a fair approximation of the changes of the EFG tensors in view of the fact that the displacements of all other atoms, as well as the orthorhombic deformations of the unit cells, were neglected. The results of the model calculations are in agreement with the symmetry properties of the system (see Sec. III), except for the fact that $\Delta V_\eta$ and $\Delta V_{xy}$ need not be zero in the AFE phase as one can see from the experimental values. In what follows no better model is needed.

Since the static probability distribution function of $W(p_l)$ of the local polarization according to the model of Refs. 4,5 is not affected by spatial short-range correlation in the deuteron, the polarization of a given bond in any unit cell can be described by the product:

$$p^i_{\mathrm{loc}}=p_{ij}\times p_l,\quad i=1,\ldots,8,\quad j=1,\ldots,6, \tag{17}$$

where $p_{ij}$ corresponds to the polarizations given in Table I and $p_l$ is a random selection out of the distribution $W(p_l)$; i.e., it runs from $-1$ to $+1$ and is weighted according to $W(p_l)$. We will now make some limiting assumptions for tractability reasons:

(i) The origin (site of the Rb probe) for which the EFG tensor is calculated is located far from the boundary of the domain or the cluster under consideration, i.e., within the observation range of this Rb nucleus we have only one Slater configuration ($j=$const).

(ii) For the case of full spatial correlation we assume that the local polarization $p_l$ is constant inside a cluster made up of a single Slater configuration but differs from cluster to cluster, so that the symmetric distribution $W(p_l)$ is reached for the whole sample without having a macroscopic polarization or sublattice polarization.

(iii) To simulate partial correlation we assume that only a fraction ($\gamma N$) of the $N$ bonds monitored by the Rb atom is ordered according to (ii), while the polarizations $p_u$ of the $(1-\gamma)N$ remaining bonds are individual selections out of $W(p)$. The number $\gamma$ is not unlike a correlation parameter ($0\le\gamma\le1$). For $\gamma=1$ the bonds are completely correlated while for $\gamma=0$ there is no correlation. In this way the ice rules are partially violated in the time average by $(1-\gamma)N$ bonds with the individual differences $p_l-p_u$.

This model is fully based on the results of the random-bond–random-field model.[4,5] With it the probability distribution of the EFG tensor elements, as well as their mutual correlations, can be calculated as a function of tem-

TABLE I. Deuteron configurations in the long-range-ordered phases. For the deuteron labeling and the direction of the O-D · · · O bonds, refer to Fig. 7.

| Configuration | $D^{(1)}$ | $D^{(2)}$ | $D^{(3)}$ | $D^{(4)}$ | $D^{(5)}$ | $D^{(6)}$ | $D^{(7)}$ | $D^{(8)}$ |
|---|---|---|---|---|---|---|---|---|
| FE 1 | + | + | + | + | + | + | + | + |
| FE 2 | − | − | − | − | − | − | − | − |
| AFE 1 | + | + | − | − | + | + | − | − |
| AFE 2 | − | − | + | + | − | − | + | + |
| AFE 3 | + | + | − | − | − | − | + | + |
| AFE 4 | − | − | + | + | + | + | − | − |

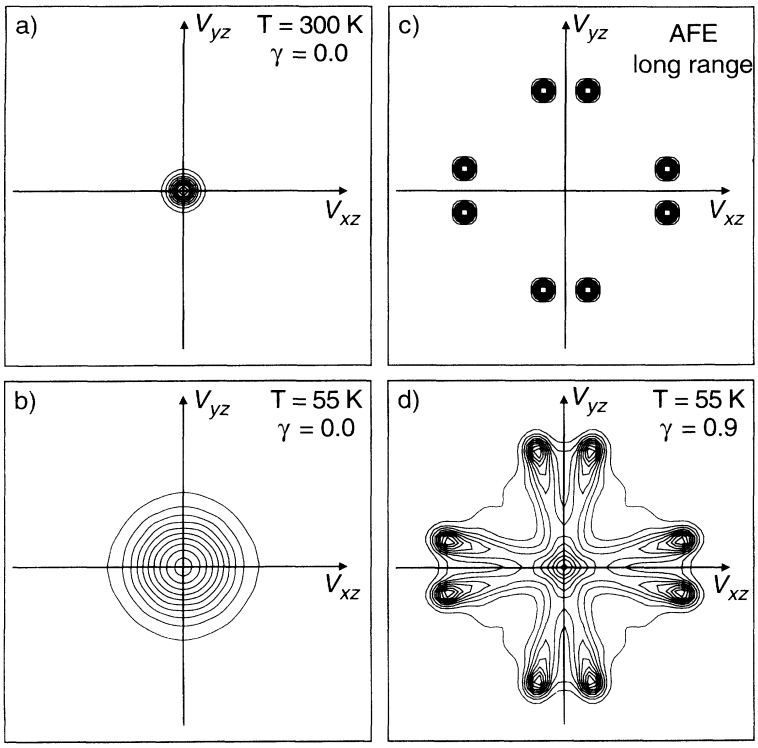


FIG. 7. Contour plots of the calculated two-dimensional histograms of the EFG tensor elements $V_{xz}$ versus $V_{yz}$ in D-RADP for different probability distributions $W(p)$ of the hydrogen-bond polarization $p$ and correlation coefficients $\gamma$. The temperature dependence of $W(p)$ is taken from Ref. 6. The eight symmetry-related EFG tensors of the AFE phase state (which corresponds to $T=0$ and $\gamma=1$) lead to the pattern (c).

perature. We are well aware that more sophisticated models which introduce the anisotropy in the correlation length in different directions are needed to describe the real situation. However, as long as we are working with the rigid-lattice model for the EFG tensors any such improvement would not lead to qualitatively different results.

Figure 7 shows contour plots of the two-dimensional histograms of $V_{xz}$ versus $V_{yz}$ for different temperatures and correlation coefficients $\gamma$. For these calculations only AFE Slater configurations were taken into account, since the glass phase consists essentially of AFE clusters (see Sec. IV C). Figures 7(a) and 7(b) show the results for completely uncorrelated deuteron freezing ($\gamma=0$) at room temperature and at 55 K, respectively. The width of the distributions is proportional to $q_{\mathrm{EA}}$, i.e., to the second moment of $W(p)$.[5–7] One can see that there is no correlation between $V_{xz}$ and $V_{yx}$ and that the distributions have Gaussian shapes as stated in the first paragraph of Sec. IV A, although $W(p)$ is clearly double peaked at 55 K.

Figure 7(c) displays correlation between $V_{xz}$ and $V_{yz}$ for long-range AFE ordering ($\gamma=1$ and $T=0$). The eight spots correspond to the eight symmetry-related EFG tensors according to Sec. III. The spots are convoluted with narrow Gaussian distributions to simulate the incoherent background. It should be noted that the experiment (AFE phase of D-RADP-95) yields a different pattern which corresponds precisely to a rotation of Fig. 7(c) by 45° and an increased distance (by 50%) between the closest spots. Figure 7(d) shows the situation for $\gamma=0.9$ and $T=55$ K. While the distribution $W(p)$ is responsible for the rims between the spots related by an inversion at the origin, the loss in spatial correlation becomes visible through the smearing of the correlation between $V_{xz}$ and $V_{yz}$.

For calculation of the NMR line shape according to Eq. (9) the needed distribution of $\Delta V_{yz}$ is obtained from a projection of the two-dimensional (2D) distribution function shown in Fig. 7(d) on the (1,0,0) plane, which contains the magnetic-field vector $\mathbf{B}_0$, for a rotation around the [1,0,0] axis. This is shown in Fig. 8(a). Similarly for the rotation axis [1,1,0] the projection has to be performed on the (1,1,0) plane, Fig. 8(b). Convoluting these distributions with a Gaussian, which corresponds approximately to the observed inhomogeneous background, yields a triple-peaked structure and a double-peaked structure for the two cases (a) and (b). This convolution takes care of the fact that a considerable fraction of Rb atoms are not far from cluster boundaries, or even within them, violating the assumption (i). For the comparison of calculated and measured spectra we have to replace the long-range calculated AFE EFG tensors by the experimental ones. This leads to changes of the spectra which can be approximated roughly by the exchange of the assignment of the rotation axes ([1,0,0] and [1,1,0]). Furthermore it shifts the two inner peaks of Fig. 8(a) outward and the two outer peaks inward by about 10%, so that the convoluted spectrum becomes a single-peaked spectrum. This was indeed observed in the [1,1,0] rotation pattern. The spectrum Fig. 8(b) is less affected by the EFG tensor replacement, since it leaves the inner peaks invariant and moves the outer peaks outward by about 10%, which does not change the double-peaked structure of the convoluted spectrum. This was observed for certain orientations of the [1,0,0] rotation pattern, Fig. 2(d).

Reducing the correlation coefficient $\gamma$ reduces the

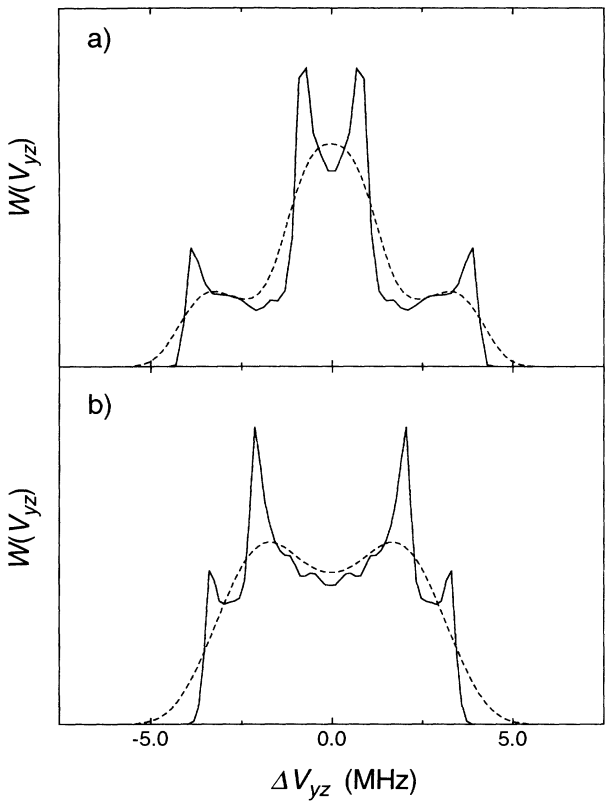


FIG. 8. Projection of the 2D distribution function shown in Fig. 8(d) on (a) the (1,0,0) plane and (b) the (1,1,0) plane. The dashed line corresponds to a convolution of the projections with a Gaussian.

peaks and fills in the minima of the spectrum progressively, so that the double-peaked convolution becomes single peaked below $\gamma = 0.8$. A similar effect is obtained when FE clusters are taken into account, because they yield always a single-peaked structure distributed around the origin. This is a further proof for the absence of FE clusters in the glass phase. It seems that FE clusters can only exist if they are large. This can be achieved only in almost ammonium-free regions of the crystal. This conclusion is supported by our investigations of the phase boundary between long-range FE and glassy order.[1]

## VI. CONCLUSIONS

We have shown that the inhomogeneous NMR line shape of $^{87}$Rb in D-RADP-50 contains information about the spatial correlation of the deuteron ordering. While uncorrelated ordering yields uncorrelated Gaussian distributions of the EFG tensor elements, a short-range correlated ordering, adhering to the ice rules within a certain correlation length, unambiguously introduces correlation between some of these elements. This correlation becomes visible in the NMR line shape as a double-peaked structure for certain orientations of the external magnetic field with respect to the crystal axes. From the temperature dependence of the NMR line shapes we know that the onset of correlated ordering begins at 150 K. From the orientation dependence we conclude that the glass phase in D-RADP-50 below 60 K consists essentially of AFE clusters with an average size of about 8 nm$^3$ which is about $\frac{1}{2}-\frac{1}{3}$ of the observation range of the Rb ($\sim$15–25 nm$^3$). This is the volume around a given Rb atom in which small changes of the charge distribution can be observed by $^{87}$Rb NMR. It should be noted that when the cluster size exceeds the size of the observation range, the NMR spectra exhibit the patterns characteristic of the long-range-ordered phase states. This is indeed observed in other regions of the phase diagram: e.g., in D-RADP-70 (Ref. 1) where the system undergoes a diffuse phase transition (local first-order phase transitions with a spatial distribution of transition temperatures) into an AFE relaxor phase, Fig. 1. The average size of the AFE clusters is about 20–40 nm$^3$ as estimated from Fig. 2(e). Since the NMR-NQR of ionically bonded probes is very sensitive to size changes in the range of 1–3 nm it is an ideal tool for the study of nanometric structures.

## ACKNOWLEDGMENTS

The authors would like to thank M. Ehrensperger for the synthesis of the fully deuterated D-RADP-50 material and the growth of the single crystals. This work was supported in part by the Swiss National Science Foundation.

[1] N. Korner, C. Pfammatter, and R. Kind, Phys. Rev. Lett. **70**, 1283 (1993).
[2] E. Courtens, J. Phys. (Paris) Lett. **43**, L199 (1982).
[3] U. T. Höchli, K. Knorr, and A. Loidl, Adv. Phys. **39**, 405 (1990).
[4] R. Pirc, B. Tadic, and R. Blinc, Phys. Rev. B **36**, 405 (1987).
[5] R. Pirc, B. Tadic, R. Blinc, and R. Kind, Phys. Rev. B **43**, 2501 (1991).
[6] R. Blinc, J. Dolinsek, R. Pirc, B. Tadic, B. Zalar, R. Kind, and O. Leichti, Phys. Rev. Lett. **63**, 2248 (1989).
[7] R. Kind, R. Blinc, J. Dolinsek, N. Korner, B. Zalar, P. Cevc, N. S. Dalal, and J. DeLooze, Phys. Rev. B **43**, 2511 (1991).
[8] R. BLinc, D. C. Ailion, B. Günther, and S. Zumer, Phys. Rev. Lett. **57**, 2826 (1986).
[9] J. Slak, R. Kind, R. Blinc, E. Courtens, and S. Zummer, Phys. Rev. B **30**, 85 (1984).
[10] A. Levstik, C. Filipic, Z. Kutnjak, I. Levstik, R. Pirc, B. Tadic, and R. Blinc, Phys. Rev. Lett. **66**, 2368 (1991).
[11] J. C. Slater, J. Chem. Phys. **9**, 16 (1941).
[12] R. A. Cowley, T. W. Ryan, and E. Courtens, Z. Phys. B **65**, 181 (1986).
[13] H. Arend, R. Perret, H. Wüest, and P. Kerkoc, J. Cryst. Growth **74**, 321 (1986).
[14] R. Kind, R. Blinc, and M. Koren, Phys. Rev. B **37**, 4864 (1988).
[15] D. I. Hoult and R. E. Richards, Proc. R. Soc. London A **334**,

311 (1975).
[16]O. Liechti, Ph.D. thesis, ETH Zurich, 1988.
[17]R. Kind, O. Liechti, R. Brüschweiler, J. Dolinsek, and R. Blinc, Phys. Rev. B **36**, 13 (1987).
[18]O. Liechti and R. Kind, J. Magn. Reson. **85**, 480 (1989).
[19]R. Blinc, S. Zumer, M. Koren, and D. C. Ailion, Phys. Rev. B **37**, 7276 (1988).
[20]R. Kind, O. Liechti, and M. Mohr, Ferroelectrics **78**, 87 (1988).
[21]R. Kind, M. Mohr, G. Schiemann, and O. Liechti, Ferroelectrics **106**, 125 (1990).
[22]A. Abragam, *The Principles of Magnetic Resonance,* in The International Series of Monographs on Physics, edited by W. C. Marshall and H. Wilkinson (Clarendon Press, Oxford, 1961).
[23]M. H. Cohen and F. Reif, in *Solid State Physics,* edited by F. Seitz and D. Turnbull (Academic, New York, 1957), Vol. 5, p. 321.
[24]B. C. Gerstein and C. R. Dybowski, *Transient Techniques in NMR of Solids* (Academic, Orlando, 1985).
[25]E. Matsushita, J. Phys. Soc. Jpn. **61**, 1336 (1991).